PAPER

Check for updates

Sensitive tear screening of diabetic retinopathy with dual biomarkers enabled using a rapid electrokinetic patterning platform†

Jen-Yi Wang,[a] Jae-Sung Kwon, [iD] *[bcd]
Sheng-Min Hsu[e] and Han-Sheng Chuang [iD] *[af]

Bead-based immunosensors have intrigued the scientific community over the past decades due to their rapid and multiplexed capabilities in the detection of various biological targets. Nevertheless, their use in the detection of low-abundance analytes remains a continuing challenge because of their limited number of active enrichment approaches. To this end, our research presents a delicate microbead enrichment technique using an optoelectrokinetic platform, followed by the detection of dual biomarkers for the sensitive screening of an eye disease termed diabetic retinopathy (DR). In this study, microbeads turned fluorescent as their surfaces formed sandwiched immunocomplexes in the presence of target antigens. The tiny fluorescent dots were then concentrated using the optoelectrokinetic platform for the enhancement of their signals. The signal rapidly escalated in 10 s, and the optimal limit of detection was nearly 100 pg mL^{-1}. For practical DR screening, two biomarkers, lipocalin 1 (LCN1) and vascular endothelial growth factor (VEGF), were used. Approximately 20 μL of analytes were collected from the tear samples of the tested patients. The concentrations of both biomarkers showed escalating trends with the severity of DR. Two concentration thresholds of LCN1 and VEGF that indicate proliferative DR were determined out of 24 clinical samples based on the receiver operating characteristic curves. For verification, a single-blind test was conducted with additional clinical tear samples from five random subjects. The final outcome of this evaluation showed an accuracy of >80%. This non-invasive screening provides a potential means for the early diagnosis of DR and may increase the screening rate among the high-risk diabetic population in the future.

Introduction

Millions of people have been recently diagnosed with diabetes mellitus (DM) worldwide, and this number continuously increases.[1] Among the population with DM, almost all patients with type 1 DM and >60% of patients with type 2 DM suffer from diabetic retinopathy (DR).[2] The high prevalence makes DR the major cause of vision impairment or blindness in patients with DM. The risk escalates with age.[3] However, the non-fatality of DR results in a low screening rate of <30%.[4,5] Current clinical diagnostic tools

for DR screening, such as fluorescence angiography (FAG) and optical coherence tomography (OCT), are limited to non-quantitative examinations and invasive diagnosis, which generally require high costs.[6,7] In addition, conventional funduscopic examination not only consumes time but also heavily relies on the personal experience of ophthalmologists. Given the abovementioned inconvenience in eye screening, non-invasive and sensitive DR diagnosis enabling the acquisition of quantitative data then becomes vital for preventing vision impairment or blindness in patients with DM. To this end, proteomic analysis has been gradually incorporated into numerous sensing devices because of its high selectivity and sensitivity with appropriate biomarkers.[8–12] Among proteomic diagnostics, the paper-based enzyme-linked immunosorbent assay (P-ELISA) is a promising tool for the rapid screening of some diseases.[13] Hsu *et al.*[14,15] reported an inexpensive and highly sensitive detection technique for proliferative DR (PDR), retinal vein occlusion, and age-related macular degeneration based on the P-ELISA diagnostic approach. They prepared 2 μL of aqueous humor from patients and mixed it with bevacizumab to react with horseradish peroxidase. Eventually, quantitative

[a] *Department of Biomedical Engineering, National Cheng Kung University, Taiwan*
[b] *Division of Thermal and Fluids Science, Institute for Computational Science, Ton Duc Thang University, Ho Chi Minh City, Vietnam. E-mail: jsungkwon@tdtu.edu.vn*
[c] *Faculty of Electrical and Electronics Engineering, Ton Duc Thang University, Ho Chi Minh City, Vietnam*
[d] *Department of Mechanical Engineering, Incheon National University, Incheon, Republic of Korea. E-mail: jsungkwon@inu.ac.kr*
[e] *Department of Ophthalmology, National Cheng Kung University Hospital, Taiwan*
[f] *Center for Micro/Nano Science and Technology, National Cheng Kung University, Taiwan. E-mail: oswaldchuang@mail.ncku.edu.tw*
† Electronic supplementary information (ESI) available. See DOI: 10.1039/c9lc00975b

colorimetric results were obtained using a cell phone camera. The limit of detection (LOD) obtained for vascular endothelial growth factor (VEGF) was as low as 33.7 fg mL^{-1}. However, variations between cell phones and calibrations upon different measurement environments remain underexplored. Walsh III et al.[16] developed a centrifugal fluidic device for immunoassays for ocular diagnosis with VEGF. This device achieves a VEGF LOD of 1 ng mL^{-1} with only a 50 μL tear sample requirement. However, the collection of such a sample size may still be a great barrier. Liu et al.[17] detected gold nanoparticles functionalized with dsDNA by forming plasmonic hotspots through glass nanocones. A final LOD readout of 1 fM was achieved. Víctor Ruiz-Valdepeñas Montiel et al.[18] used a magnetic bead-based immunosensor for the detection of alpha-lactalbumin, a human allergen. A sandwiched immunocomplex involving selective capture and detector antibodies was formed on the magnetic beads, and the detection relied upon a hydroquinone/H$_2$O$_2$ system. An LOD of 11 pg mL^{-1} was reached. High flexibility and ease of incorporation into another system make the bead-based bioassay a promising platform for trace amount detection. Nevertheless, sophisticated equipment is required to drive the magnetic system. In general, all existing techniques focus on a single target analyte only, resulting in potential uncertainty in specificity.

In the present study, a non-invasive immunosensing technique (Fig. 1) based on an optoelectrokinetic platform, termed rapid electrokinetic patterning (REP),[19–24] was used to manipulate immunocomplexed microbeads for the detection of DR biomarkers in tear samples. We utilized a colloidal suspension containing microbeads conjugated with capture and free suspending fluorescence tagged probe antibodies. When the colloidal suspension was well mixed and incubated with a tear sample, sandwiched immunocomplexes would form on the microbeads in the presence of target antigens. The formation of the sandwiched immunocomplexes leads to primary signal enrichment. Notably, the fluorescence intensity of the microbeads was dose dependent. The intensity was further enhanced by secondary signal enrichment by concentrating the dispersed microbeads with REP. The final signal intensity of the REP-driven concentration was two-fold higher than that of sole sandwiched immunocomplexes and nearly six-fold higher than that without enrichment (Fig. S1, ESI†). The multiple signal enrichment allowed the proposed technique to achieve an LOD as low as 100 pg mL^{-1}, which was vital to detect low-abundance analytes in tear samples. For specific diagnosis, two biomarkers rather than one were separately used herein for DR diagnosis. Several potential biomarkers in tear proteins, such as LCN1, TNF-a, VEGF, and beta-2 microglobulin (B2M), have been suggested for DR diagnosis.[25–28] Among the biomarkers, LCN1 and VEGF are two proteins that are rich in tear film and highly correlate with DR. Both biomarkers have been regarded as good indicators of DR in tears[29] and were selected in this study. The severity of DR escalates with their concentrations. The thresholds for LCN1 and VEGF in healthy tear samples are approximately 1–2 mg mL^{-1} and 1 ng mL^{-1}, respectively.[30–32] Accordingly, 20 μL of non-stimulated tear sample was collected from each patient, whereas only 1.5 μL was required for a single measurement. The minimum volume of the tear sample, 1.5 μL, was experimentally determined by our previous study.[33] By investigating tear samples from 24 clinical volunteer subjects, the estimated concentration thresholds of LCN1 and VEGF for PDR were approximately 250 μg ml^{-1} and 10 ng ml^{-1} based on the receiver operating characteristic (ROC) curves, respectively. With this standard, a single-blind test was conducted with five additional clinical tear samples to verify the feasibility of the technique. The evaluation showed an accuracy of >80% for PDR detection on the system. This approach successfully demonstrated the sensitive screening of DR with the two biomarkers. Similarly, this technique can be applied to other tear screenings of diseases in the future by simply replacing their corresponding capture and probe antibodies.

Materials and methods

Bead-based sandwiched immunoassay

Sandwiched immunocomplexes were designed to form on the surfaces of amine-modified polystyrene (PS) microbeads (17145-5, Polysciences) in the presence of LCN1 (H00003933-M02, Abnova) or VEGF (900-M10, Peprotech). The immunocomplex formation was visualized from the secondary antibody labelled with a green and orange fluorophore (A21206/R37119, Invitrogen). The sandwiched configuration was composed of a capture antibody (monoclonal mouse anti-LCN1 IgG/monoclonal mouse anti-VEGF IgG), a target antigen (LCN1/VEGF), and a probe antibody (polyclonal rabbit anti-LCN1 IgG/polyclonal rabbit anti-VEGF IgG). In the preparation of each sample, 1-ethyl-3-(3-dimethylaminopropyl)-carbodiimide (A10807, Alfa Aesar) and N-hydroxysuccinimide (6066-82-6, Sigma) were first added to 2-(N-morpholino) ethanesulfonic acid (M3671, Sigma) buffer to activate the carboxyl groups on the capture
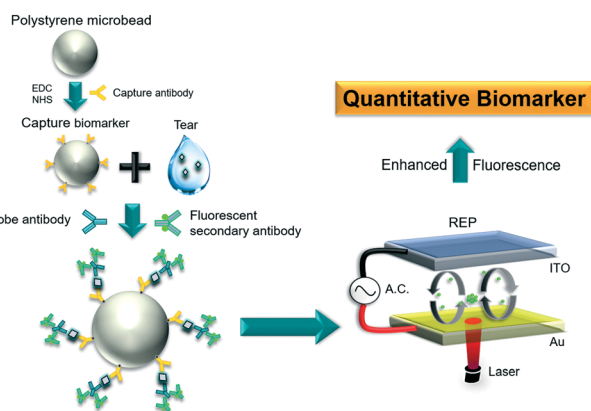

Fig. 1 Conceptual schematic of the tear screening of DR on an optoelectrokinetic platform.

antibody. As a result, the antibody was conjugated with the amine-modified PS microbeads. The mixture was incubated in a thermal shaker at 800 rpm and 4 °C for 4 h for the completion of the conjugation. The free suspending antibodies were washed away by three centrifugation steps. In addition, PEG4000 (A16121, Alfa Aesar) was used as a blocking reagent to prevent nonspecific binding.

Before the reaction, 1.5 μL of tear sample for LCN1 was diluted 100-fold with 1× PBS + 0.1% Tween 20 (PBST) washing buffer. By contrast, the tear sample for VEGF required no dilution. Subsequently, the tear sample was mixed with the capture antibody-conjugated microbeads and incubated at 800 rpm and 25 °C for 1 h. Extra analytes were washed with PBST by three centrifugation steps. Afterward, the solutions were mixed and incubated with the probe antibody (rabbit polyclonal anti-LCN1/VEGF IgG) at 800 rpm and 25 °C for 1 h. For subsequent visualization, the probe antibody was further conjugated with additional dye (488/594) tagged (A21206/R37119, Invitrogen) with a secondary antibody to express the presence of the corresponding biomarkers in the test media. In the last step, the buffer was replaced with deionized water to lower the electrical conductivity below 1 mS m^{-1}.[34] Notably, low conductivity was required for the normal operation of REP.

Chip fabrication

The chip used for the REP-based detection and screening of LCN1 and VEGF biomarkers comprised two electrode plates separated with a 110 μm spacer. The bottom plate was fabricated by coating 30 nm Cr as an adhesive layer and 150 nm Au as a conductive layer on a glass substrate. By contrast, the top plate was a commercial ITO glass that provided a transparent window for visualization. Prior to measurements, only 1 μL of the mixed sample droplet (i.e., tear, microbeads, and reagents) was sandwiched between the two parallel electrode plates which were then clamped with magnets. Notably, unlike the 1.5 μL of tear sample, the 1 μL here is the minimum volume of the final mixed sample droplet to be detected on our platform. During operation, an AC signal was supplied to the electrodes to allow electrical current to run through the aqueous droplet, inducing the subsequent optoelectrokinetic effect.

Optoelectrokinetic platform and microbead manipulation

The signal enrichment for biomarker detection was achieved using a self-established optoelectrokinetic platform, termed REP (Fig. 2). The chip was placed on an upright epifluorescence microscope (BX51, Olympus) for microbead manipulation. A driving voltage generated from an alternating current (AC) signal source (FG-3015, GWINSTE) and amplified using a power amplifier (2340, TEGAM) was supplied to the electrodes of the chip. In addition, an infrared laser beam (300 mW, 1064 nm, LD-WL206, Optoelectronics Tech.) was focused on the bottom gold electrode. The electric voltage produces electrostatic force to
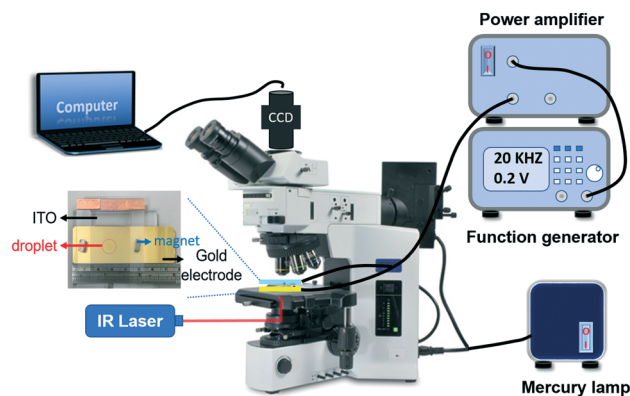

Fig. 2 Experimental setup of the REP platform. The inset illustrates the chip used for bead manipulation by REP.

attract suspended microbeads to the bottom electrode. Laser irradiation creates a local temperature gradient in the sample droplet to generate AC electrothermal toroidal (ACET) vortex under electric voltage.[35,36] The ACET vortex sweeps the attracted microbeads toward the irradiated laser spot, whereas the electrostatic force lets the beads remain at the bottom electrode. Thus, ACET flow and electrostatic force play a major role in concentrating microbeads for biomarker detection.

The fluorescence intensity of the microbeads was enhanced as they are concentrated by REP. We previously showed that microbead manipulation is a function of electrical frequency.[20,24,34] In this study, the optimal manipulation of 3 μm microbeads by REP was realized with 15 V$_{pp}$ at 35 kHz and 12 mW laser intensity. The fluorescence of the microbeads dynamically aggregated under the operating conditions was excited and emitted through a filter cube equipped in the microscope. The fluorescence images were acquired using a digital camera (FL3-03-13S2C-CS, Point Grey) and then stored in a computer for data analysis.

Determination of thresholds for biomarkers

Specificity, sensitivity, and accuracy are the major concerns in the determination of the thresholds for LCN1 and VEGF. As a result, the ROC curve was employed here to optimize the determination. The data were acquired from clinical tear samples to ensure that the thresholds selected were feasible for actual clinical screening. For simplicity, only two groups, namely, PDR and non-PDR, were classified. Notably, the non-PDR group may include healthy subjects and patients with non-proliferative DR (NPDR) or other non-DR ocular diseases. In an ROC diagram, the upper-leftmost corner represents the ideal situation, which implies 100% sensitivity, specificity, and accuracy. However, given that the ideal case is nearly impossible in reality, an optimal alternative was sought to find a point that connects the shortest distance between the corner and the curve. Eventually, the alternative point defined a reasonable outcome to balance the specificity, sensitivity, and accuracy in the measurement.

Results and discussion

Effects of bead-based immunoassays with LCN1 and VEGF

LCN1 and VEGF are two tear proteins associated with the severity of DR. LCN1 belongs to the lipocalin family of extracellular proteins that may bind to hydrophobic ligands and inhibit cysteine proteinases. VEGF mainly facilitates the growth of neovascularization. The concentration levels of LCN1 and VEGF increase as DR progresses. Therefore, DR can be screened by monitoring the variations in both biomarkers. The specificity of DR screening can be enhanced when the biomarkers are simultaneously used. To this end, the specificity characteristics of LCN1 and VEGF were verified individually (Fig. 3). Only the corresponding target proteins of anti-LCN1 and anti-VEGF capture antibodies were detected and expressed with fluorescence. The nonspecific binding was much lower than that of their specific counterparts and similar to that of the control. The low nonspecific binding provided a good foundation for the detection of dual biomarkers.

The dose-dependent fluorescence intensity of LCN1 and VEGF was calibrated (Fig. 4). The intensity was expressed as the relative ratio of the difference between the experimental and control values to the control value. The relative fluorescence intensity was obtained over a broad range of concentrations from 100 pg mL^{-1} to 10 μg mL^{-1}, covering five orders of magnitude. The corresponding fluorescence signal increased with the concentration of the target proteins. By finding the intersection of the threefold error bars of the control and the linear trend line, the estimated LOD level for both biomarkers was 100 pg mL^{-1}.

Screening thresholds of LCN1 and VEGF from clinical samples

The thresholds of the DR biomarkers must be determined prior to the clinical diagnosis of DR. Although 1–2 mg mL^{-1} and 1 ng mL^{-1} were reported[29–31] as critical concentration levels of LCN1 and VEGF in healthy human tears,

Fig. 4 Calibrations of relative intensity with respect to different concentrations of (A) LCN1 and (B) VEGF ranging from 100 pg mL^{-1} to 10 μg mL^{-1}. The symbols "*", "**", and "***" denote $p < 0.05$, $p < 0.01$, and $p < 0.001$, respectively, under Student's t test ($n = 4$). The error bars represent standard deviations.

respectively, the levels may still vary according to the sample preparation method. As a result, the ROC curve was used herein in the determination of the appropriate thresholds of the two biomarkers in our system (Fig. 5A). According to a graphical guideline, an optimal point on the curve was connected to the upper left corner with the shortest distance, which also implied the best combination of specificity and selectivity. The optimal points were selected from the data of LCN1 and VEGF levels obtained from 24 volunteers, including 8 healthy subjects, 13 patients with PDR, 2 patients with NPDR, and 1 patient with glaucoma based on the ROC curve (Fig. S2, ESI†). The volunteers were classified into two categories, PDR and non-PDR groups, depending on their HbA1c blood tests and clinical examinations by our collaborative ophthalmologist. Tear sample collection was conducted by another clinical specialist at the Department of Ophthalmology, National Cheng Kung University Hospital (NCKUH) under an IRB agreement # A-ER-105-113. The patients were selected by the ophthalmologist in advance. Exclusion criteria included dry eye syndrome, macular
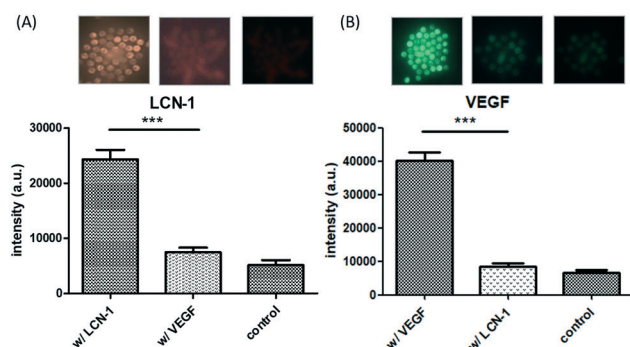
Fig. 3 Specificity of LCN1 and VEGF. Fluorescence intensity values of (A) anti-LCN1 and (B) anti-VEGF conjugated microbeads in the presence of different antigens ($n = 4$). The top insets showing fluorescent particle images correspond to the bottom bar chart.
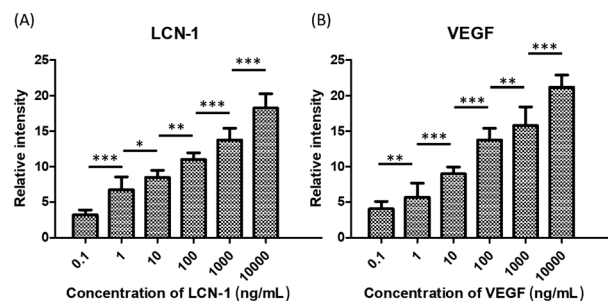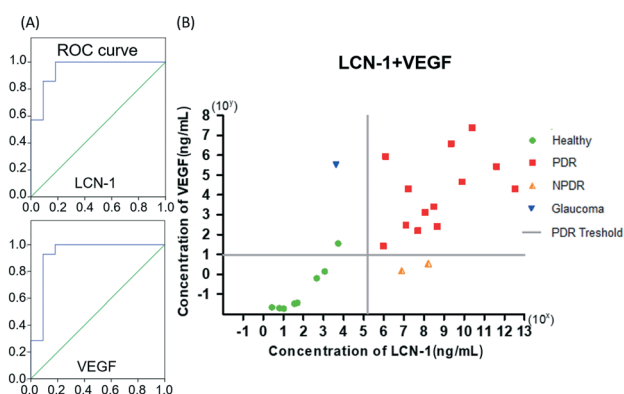
Fig. 5 (A) ROC curves of LCN1 and VEGF depending on 24 clinical samples. (B) Concentration distribution of 24 clinical data, which are expressed in terms of the concentrations of LCN1 and VEGF. Each of the two solid lines represents the thresholds of LCN1 (vertical line) and VEGF (horizontal line). Colors of the data points represent the health conditions according to the clinical diagnostic reports.

degeneration, under drug treatments, and below 45 years of age. Tear samples were obtained through a glass capillary. First, the lower lid was pulled downward, revealing the conjunctival sac into which the glass capillary was held horizontally. Owing to the capillary effect, the tear fluid then flowed into the glass capillary. Finally, the tear sample was pipetted out of the glass capillary into a microcentrifuge tube and stored in a refrigerator for later use.

For a simple judgement, a concentration distribution graph of all 24 participants with respect to the two selected biomarkers is plotted in Fig. 5B. Based on the ROC curve mentioned previously, the 24 tear samples provided two baselines as thresholds. The final threshold values of LCN1 and VEGF on the platform were approximately 250 μg ml^{-1} and 10 ng ml^{-1}, respectively. Notably, the threshold of LCN1 for PDR was lower than that previously mentioned. The discrepancy was very likely due to the multiple dilutions. Thus, the original concentration may not be linearly proportional to the dilution ratio. Despite the mismatch in the absolute value, the screening method was reliable as long as the diagnosis was performed on the same system. In the graph, the vertical and horizontal solid lines represent the thresholds of LCN1 and VEGF for PDR, respectively. When the diagram was divided into four sections with two solid lines, the data lying in the first quadrant could be classified as severe PDR. The severity escalates as the data point moves to the upper-rightmost corner. Conversely, the data in the third quadrant stand for healthy subjects. Apart from the above two cases, the data in the second and fourth quadrants usually imply potential concerns in other diseases associated with LCN1 (NPDR) and VEGF (glaucoma). These exceptional cases suggested the necessity of dual biomarkers for DR screening to achieve high specificity of diagnosis. Notably, for data that are close to the boundary lines of the first quadrant, the proximity may imply a high risk of progressing to PDR. Thus, the patient requires immediate medical intervention. An exceptional green dot corresponding to a healthy person is located near the boundary of the second quadrant. This case was later identified as a person with a family history of diabetes. Accordingly, this abnormal index may be an early sign of potential DR in the future. Finally, this diagram provided a reliable graphical guideline for diagnosing PDR in unknown subjects. The accuracy of each single biomarker was approximately 88.5%, whereas that of dual biomarkers reached up to nearly 100%. As a result, the use of dual biomarkers was of great help in improving the accuracy of DR detection.

Evaluation of the optoelectrokinetic platform with single-blind tests

By referring to the distribution graph established previously, we performed single-blind DR screening with the optoelectrokinetic platform to evaluate the feasibility of this technique in actual clinical practices. In the tests, five unknown patients were first selected and examined by an ophthalmologist at the NCKUH. PDR patients may or may
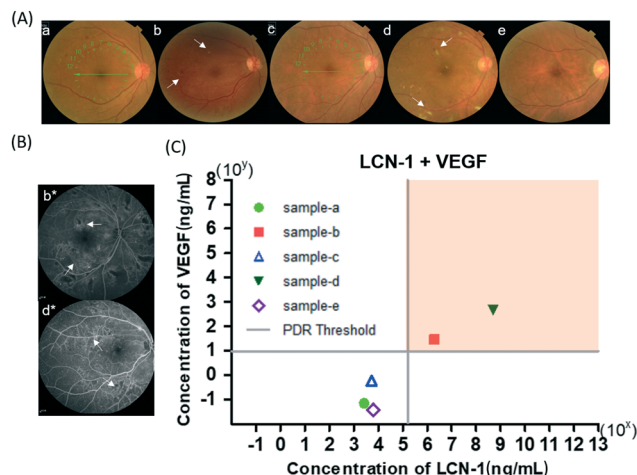

Fig. 6 (A) Funduscopic micrographs of five unknown patients. The insets a, b, and d are samples from patients with PDR while the insets c and e are samples from healthy subjects. The arrows in b and d indicate the bleeding spots. (B) Fluorescein angiography images from the patients with PDR. b* and d* are labels corresponding to the previous micrographs b and d, respectively. The arrows indicate the bleeding spots. (C) Concentration distribution of the single-blind tests. The solid lines define the thresholds of LCN1 and VEGF for PDR. The hollow icons represent healthy subjects, whereas the solid icons represent the patients with PDR according to their clinical reports. The upper right region filled with orange color is the suggested PDR domain based on the ROC analysis.

not be present among the subjects. All of them underwent a blood test and conventional ocular examination (Fig. 6A). Subsequently, two of the examinees (b and d) had severe PDR, and their abnormal bleeding spots were indicated by the white arrows in the fluorescein angiography images (Fig. 6B). Notably, examinee (a) was diagnosed with PDR three years ago but fully recovered after a laser treatment. The remaining two examinees (c and e) were confirmed to be free from any DR symptoms. By contrast, our measurements were plotted in the distribution graph according to the concentrations of LCN1 and VEGF (Fig. 6C). Clearly, samples (b) and (d) were in the PDR region, whereas the three other samples (a), (c), and (e) fell within the healthy region. The comparison of the two results indicated that the screening accuracy on the REP platform was 80%. However, for sample (a), which was fully recovered from PDR and was now a clinically healthy case, the discrepancy with our measurement may be debatable. For further information, the detailed comparison is presented in Table 1.

Table 1 Result of the single-blind tests

	LCN-1	VEGF	Our REP system	Hospital results	P.S.
Patient a	✗	✗	Negative	Positive	The patient was cured after treatments
Patient b	✓	✓	Positive	Positive	
Patient c	✗	✗	Negative	Negative	
Patient d	✓	✓	Positive	Positive	
Patient e	✗	✗	Negative	Negative	

Conclusions

DR has recently become a common complication of diabetes, which is a rapidly growing metabolic disease. Nevertheless, DR receives little attention from the public because of its non-fatality. This universal negligence results in a worldwide low screening rate of <30%.[4,5] The root causes of this condition may be attributed to the inconvenience of current clinical screening procedures, such as fear of invasive examinations (*e.g.*, FAG), unreliability due to non-quantitative diagnosis, and high cost for some new diagnostic instruments, such as OCT. To address these obstacles, we proposed a technique combining an optoelectrokinetic platform and a bead-based immunoassay for the sensitive screening of DR with two DR biomarkers, LCN1 and VEGF, in human tears. The preliminary results showed high specificity and linear dose-dependent responses. A broad range of measurements over five orders of magnitude and an LOD of as low as 100 pg mL^{-1} were achieved. In the preparation of the method for actual clinical screening, the ROC curve was used to determine the optimal thresholds of LCN1 and VEGF for PDR on 24 clinical tear samples. A minimum of 1.5 μL of tear sample was needed for each measurement. With a sensitivity of 92.9%, a specificity of 90.9%, and an accuracy of 88.46%, the thresholds of LCN1 and VEGF measured with the technique were 250 μg mL^{-1} and 10 ng mL^{-1}, respectively. On the basis of the fine-tuned parameters, we conducted single-blind tests with five unknown tear samples selected by our collaborative ophthalmologist. By comparing the measurements with their clinical diagnoses, we achieved an accuracy of at least 80%. Among the participants, two were confirmed to have PDR, two were healthy individuals free from any DR symptoms, and the remaining one was a fully recovered patient with a history of PDR. Except for the last ambivalent case, good agreement between the measurements and their clinical counterparts was obtained. Further clinical tests are expected to be conducted to minimize the uncertainty by expanding the database. Nevertheless, the technique provided a valuable solution to overcome the current deficiency in DR screening. We expect that with additional clinical samples, the proposed technique can provide insight into improving the low DR screening rate in the near future.

Author contributions

Han-Sheng Chuang: conceptualization, project administration, supervision, funding acquisition, writing – original draft, review & editing. Jen-Yi Wang: data curation, investigation, methodology, formal analysis, writing – original draft, review & editing. Jae-Sung Kwon: project administration, supervision, funding acquisition, writing – original draft, review & editing. Sheng-Min Hsu: writing – review & editing.

Conflicts of interest

There are no conflicts of interest to declare.

Notes and references

1   L. Guariguata, D. R. Whiting, I. Hambleton, J. Beagley, U. Linnenkamp and J. E. Shaw, *Diabetes Res. Clin. Pract.*, 2014, **103**, 137–149.
2   D. S. Fong, L. Aiello, T. W. Gardner, G. L. King, G. Blankenship, J. D. Cavallerano, F. L. Ferris and R. Klein, *Diabetes Care*, 2004, **27**, S84–S87.
3   E. J. Duh, J. K. Sun and A. W. Stitt, *JCI Insight*, 2017, **2**, e93751.
4   P. H. Scanlon, *Curr. Diabetes Rep.*, 2017, **17**, 96–96.
5   J. B. Skaggs, X. Zhang, D. J. Olson, S. Garg and R. M. Davis, *N. C. Med. J.*, 2017, **78**, 121–123.
6   D. Huang, E. A. Swanson, C. P. Lin, J. S. Schuman, W. G. Stinson, W. Chang, M. R. Hee, T. Flotte, K. Gregory and C. A. Puliafito, et al., *Science*, 1991, **254**, 1178.
7   S. Dithmar and F. G. Holz, *Fluorescence angiography in ophthalmology*, Springer Science & Business Media, 2008.
8   T. Wei, W. Tu, B. Zhao, Y. Lan, J. Bao and Z. Dai, *Sci. Rep.*, 2014, **4**, 3982.
9   L. B. Sagle, L. K. Ruvuna, J. A. Ruemmele and R. P. Van Duyne, *Nanomedicine*, 2011, **6**, 1447–1462.
10 K. M. Mayer, S. Lee, H. Liao, B. C. Rostro, A. Fuentes, P. T. Scully, C. L. Nehl and J. H. Hafner, *ACS Nano*, 2008, **2**, 687–692.
11 Y. Ishige, M. Shimoda and M. Kamahori, *Biosens. Bioelectron.*, 2009, **24**, 1096–1102.
12 A. Zengin, U. Tamer and T. Caykara, *J. Mater. Chem. B*, 2015, **3**, 306–315.
13 M.-Y. Hsu, C.-C. Chiu, J.-Y. Wang, C.-T. Huang, Y.-F. Huang, J.-C. Liou, C. Chen, H.-C. Chen and C.-M. Cheng, *Nanomaterials*, 2018, **8**, 310.
14 M.-Y. Hsu, S.-J. Chen, K.-H. Chen, Y.-C. Hung, H.-Y. Tsai and C.-M. Cheng, *Lab Chip*, 2015, **15**, 2357–2363.
15 M.-Y. Hsu, C.-Y. Yang, W.-H. Hsu, K.-H. Lin, C.-Y. Wang, Y.-C. Shen, Y.-C. Chen, S.-F. Chau, H.-Y. Tsai and C.-M. Cheng, *Biomaterials*, 2014, **35**, 3729–3735.
16 D. I. Walsh Iii, G. J. Sommer, U. Y. Schaff, P. S. Hahn, G. J. Jaffe and S. K. Murthy, *Lab Chip*, 2014, **14**, 2673.
17 L. Liu, N. Xia, H. Liu, X. Kang, X. Liu, C. Xue and X. He, *Biosens. Bioelectron.*, 2014, **53**, 399–405.
18 V. Ruiz-Valdepeñas Montiel, S. Campuzano, R. M. Torrente-Rodríguez, A. J. Reviejo and J. M. Pingarrón, *Food Chem.*, 2016, **213**, 595–601.
19 C. Y. Chung, J. C. Wang and H. S. Chuang, *PLoS One*, 2016, **11**, 15.
20 J.-C. Wang, H.-Y. Ku, D.-B. Shieh and H.-S. Chuang, *Biomicrofluidics*, 2016, **10**, 014113.
21 D. Han and J.-K. Park, *Lab Chip*, 2016, **16**, 1189–1196.
22 J.-S. Kwon, S. P. Ravindranath, A. Kumar, J. Irudayaraj and S. T. Wereley, *Lab Chip*, 2012, **12**, 4955.

23 J.-S. Kwon and S. T. Wereley, *J. Fluids Eng.*, 2013, **135**, 021306.

24 K.-C. Wang, A. Kumar, S. J. Williams, N. G. Green, K. C. Kim and H.-S. Chuang, *Lab Chip*, 2014, **14**, 3958–3967.

25 H. J. Kim, P. K. Kim, H. S. Yoo and C. W. Kim, *Clin. Biochem.*, 2012, **45**(1–2), 60–67.

26 D. Kim, J. Shim, H. S. Chuang and K. C. Kim, *Biomicrofluidics*, 2015, **9**, 034102.

27 C. Costagliola, V. Romano, M. De Tollis, F. Aceto, R. dell'Omo, M. R. Romano, C. Pedicino and F. Semeraro, *Mediators Inflammation*, 2013, **2013**, 629529.

28 Y. Zhao, M. Cao, J. F. McClelland, Z. Shao and M. Lu, *Biosens. Bioelectron.*, 2016, **85**, 261–266.

29 J. M. Tiffany, *Dev. Ophthalmol.*, 2008, **41**, 1–20.

30 É. Csősz, P. Boross, A. Csutak, A. Berta, F. Tóth, S. Póliska, Z. Török and J. Tőzsér, *J. Proteomics*, 2012, **75**, 2196–2204.

31 L. Zhou, S. Z. Zhao, S. K. Koh, L. Chen, C. Vaz, V. Tanavde, X. R. Li and R. W. Beuerman, *J. Proteomics*, 2012, **75**(13), 3877–3885.

32 R. J. Fullard and D. M. Kissner, *Curr. Eye Res.*, 1991, **10**, 613–628.

33 J. C. Wang, H. Y. Ku, T. S. Chen and H. S. Chuang, *Biosens. Bioelectron.*, 2016, **89**, 701–709.

34 J.-C. Wang, H.-Y. Ku, T.-S. Chen and H.-S. Chuang, *Biosens. Bioelectron.*, 2017, **89**, 701–709.

35 J.-S. Kwon and S. T. Wereley, *Microfluid. Nanofluid.*, 2015, **19**, 609–619.

36 S. Lee, J. Kim, S. T. Wereley and J.-S. Kwon, *J. Micromech. Microeng.*, 2019, **29**, 017003.